# Disordered hyperuniformity in two-component nonadditive hard-disk plasmas

Enrique Lomba,[1,2] Jean-Jacques Weis,[3] and Salvatore Torquato[2,4]
[1]*Instituto de Química Física Rocasolano, CSIC, Calle Serrano 119, E-28006 Madrid, Spain*
[2]*Department of Chemistry, Princeton University, Princeton, New Jersey 08544, USA*
[3]*Université de Paris-Sud, Laboratoire de Physique Théorique, UMR8627, Bâtiment 210, 91405 Orsay Cedex, France*
[4]*Princeton Institute for the Science and Technology of Materials, Princeton University, Princeton, New Jersey 08544, USA*
(Received 25 October 2017; published 18 December 2017)

We study the behavior of a classical two-component ionic plasma made up of nonadditive hard disks with additional logarithmic Coulomb interactions between them. Due to the Coulomb repulsion, long-wavelength total density fluctuations are suppressed and the system is globally hyperuniform. Short-range volume effects lead to phase separation or to heterocoordination for positive or negative nonadditivities, respectively. These effects compete with the hidden long-range order imposed by hyperuniformity. As a result, the critical behavior of the mixture is modified, with long-wavelength concentration fluctuations partially damped when the system is charged. It is also shown that the decrease of configurational entropy due to hyperuniformity originates from contributions beyond the two-particle level. Finally, despite global hyperuniformity, we show that in our system the spatial configuration associated with each component separately is not hyperuniform, i.e., the system is not "multihyperuniform."

DOI: 10.1103/PhysRevE.96.062126

## I. INTRODUCTION

Disordered hyperuniform systems have gained considerable attention over the last decade, since their relevance as distinguishable states of matter was first stressed by Torquato and Stillinger [1]. Hyperuniform many-body systems are those characterized by an anomalous suppression of density fluctuations at long wavelengths relative to those in typical disordered systems such as ideal gases, liquids, and structural glasses. More precisely, by definition, a hyperuniform many-particle system in $d$-dimensional Euclidean space $\mathbb{R}^d$ at number density $\rho$ is one in which the structure factor $S(\mathbf{Q}) \equiv 1 + \rho\tilde{h}(\mathbf{Q})$ tends to zero as the wave number $Q \equiv |\mathbf{Q}|$ tends to zero [1],

$$\lim_{Q\to 0} S(\mathbf{Q}) = 0, \tag{1}$$

where $\tilde{h}(\mathbf{Q})$ is the Fourier transform of the total correlation function $h(\mathbf{r}) = g_2(\mathbf{r}) - 1$ and $g_2(\mathbf{r})$ is the pair correlation function.

All perfect crystals and perfect quasicrystals, and certain special disordered systems, are hyperuniform [1,2]. The fact that the microscopic structure of disordered hyperuniform systems lie somewhere between that of disordered fluids (with only short-range disorder) and crystals (with long-range translational and orientational order) has been found to have relevant consequences in a variety of contexts and applications across different fields. This includes maximally random jammed hard-particle packings [3], classical disordered ground states [2,4–6], driven nonequilibrium granular and colloidal systems [7–9], dynamical processes in ultracold atoms [10], photonic band-gap materials [11–13], dense disordered transparent dispersions [14], photoreceptor mosaics in avian retina [15], immune system receptors [16], composites with desirable transport, dielectric, and fracture properties [17–20], polymer-grafted nanoparticle systems [21], and "perfect" glasses [6].

Our fundamental understanding of disordered hyperuniform systems is still in its infancy. We know that one can achieve them via equilibrium and nonequilibrium routes, and they come in quantum-mechanical and classical varieties. Classical disordered hyperuniform systems of identical particles in equilibrium necessarily possess long-range interparticle interactions, whether they occur at ground-state ($T = 0$) conditions [2,4–6] or positive temperatures [22,23]. However, much less is known about the hyperuniformity of classical multicomponent systems, and yet the infinite parameter space (particle size distribution and composition) afforded by them should provide greater tunabililty to achieve hyperuniform states. Of course, when more than one component is present in the system, the situation becomes obviously more involved, but also physically more interesting, including technological relevance as designer composites [17–20].

It is noteworthy that when there are two or more components, the system can be globally hyperuniform (long-wavelength total density fluctuations are suppressed) or *multihyperuniform* (long-wavelength density fluctuations are suppressed for each and every component). In practice, multihyperuniformity in this case amounts to suppressing simultaneously long-wavelength total density and concentration fluctuations. These possibilities are accounted for by the Bhatia-Thornton structure factors [24]. In the first instance, one must consider the total structure factor $S_{\mathrm{NN}}(Q)$, defined as

$$S_{\mathrm{NN}}(Q) = \sum_{\alpha\beta} S_{\alpha\beta}(Q), \tag{2}$$

where the partial structure factors, $S_{\alpha\beta}(Q)$, are given by

$$S_{\alpha\beta}(Q) = x_\alpha\delta_{\alpha\beta} + \rho x_\alpha x_\beta \tilde{h}_{\alpha\beta}(Q), \tag{3}$$

where $x_\alpha$ is the mole fraction of component $\alpha$, $\delta_{\alpha\beta}$ Kronecker's delta, $\rho$ the total number density, and $\tilde{h}_{\alpha\beta}(Q)$ the Fourier transform of the total partial correlation function [$h_{\alpha\beta}(r) = g_{\alpha\beta}(r) - 1$, where $g_{\alpha\beta}$ is the partial pair distribution function]. The low-$Q$ behavior of the total structure factor is connected to

 

the isothermal compressibility of the systems, and it is known to diverge when the critical point of a liquid-vapor transition is approached (i.e., density fluctuations occur on the macroscopic length scale). A hyperuniform system is the antithesis of such a critical point with a total structure factor that vanishes in this low-$Q$ limit according to (1) but can be regarded to be at an "inverted" critical point in which the direct correlation function, defined through the Ornstein-Zernike equation, becomes long-ranged [1]. Additionally, concentration fluctuations are described by the concentration-concentration structure factor, defined by [24,25]

$$S_{cc}(Q) = x_2^2 S_{11}(Q) + x_1^2 S_{22}(Q) - 2x_1 x_2 S_{12}(Q). \quad (4)$$

This quantity exhibits a low-$Q$ divergence when the binary system approaches the consolute point, i.e., the demixing critical point. Conversely, if the system is globally hyperuniform, multihyperuniformity implies the suppression of low-$Q$ concentration fluctuations:

$$\lim_{Q\to 0} S_{cc}(Q) = 0. \quad (5)$$

In this paper, we theoretically and computationally investigate the behavior of 2D classical two-component ionic plasmas made up of nonadditive hard disks with additional logarithmic Coulomb interactions between them. By a two-component ionic plasma we refer to a mixture of two different positively charged species in a neutralizing background of negative charge [26]. We will show that due to the Coulomb repulsion, long-range total density fluctuations are suppressed and the systems are globally hyperuniform at positive temperatures. It is demonstrated that short-range volume effects lead to phase separation or to heterocoordination for positive or negative nonadditivities, respectively. Interestingly, we show that the decrease of configurational entropy due to hyperuniformity originates from contributions beyond the two-particle level. Finally, despite global hyperuniformity, we show that in our system the structure of each component separately is not hyperuniform, i.e., the system is not "multihyperuniform." We note here, that even though our model interaction is strictly a mathematical construct resulting from 2D electrodynamics, it can also be thought as an effective coarse-grained model for much more complex realistic systems. In fact, the experimental structure factors obtained from the distribution of avian photoreceptors in Ref. [15] show a linear and/or quadratic dependence in the low-wave number regime. This actually amounts to effective interactions that display either an inverse power or logarithmic $r$ dependence, i.e., effective three-dimensional (3D) repulsive Coulomb in a plane $(1/r)$, or two-dimensional (2D) repulsive Coulomb $(-\log r)$. Concerning the results presented in this work, it is worth mentioning that a qualitatively similar picture from the point of view of hyperuniformity would have been obtained had the Coulomb interaction been fully 3D (i.e. $\propto 1/r$), with the particles constrained to lie on a plane. The only relevant difference would be a linear decay of $S_{NN}(Q)$ as $Q \to 0$, instead of the quadratic dependence, induced by the logarithmic dependence, shown in Eq. (36) below.

Here more specifically we will study one of the simplest disordered binary systems that can exhibit hyperuniformity in two dimensions, namely, the symmetric nonadditive hard-disk (NAHD) plasma. This system is characterized by a short-range NAHD interaction, to which a long-range repulsive 2D Coulomb interaction is superimposed. As mentioned before, the 2D Coulomb potential in plasma systems is known to lead to hyperuniformity [27–29], with $\lim_{Q\to} S(Q) \propto Q^2$. On the other hand, the short-range part of the potential for positive nonadditivity [i.e., when $\sigma_{\alpha\beta} > (\sigma_{\alpha\alpha} + \sigma_{\beta\beta})/2$, where $\sigma_{\alpha\beta}$ is the distance of minimum approach between particles $\alpha$ and $\beta$] can induce a demixing transition [30,31]. In contrast, for negative nonadditivities, the system will be fully miscible and presents a tendency to heterocoordination, i.e., local coordinations with neighboring unlike particles tend to be favored. Our study makes extensive use of Monte Carlo (MC) simulations and integral-equation approaches, namely, the Hypernetted Chain (HNC) equation and the closely related Reference Hypernetted Chain equation (RHNC). With these tools, we investigate the structural effects of the interplay between long- and short-range interactions, with special emphasis on the influence of hyperuniformity on the critical behavior of the demixing transition for the NAHD plasma with positive nonadditivity. This is a particularly interesting situation, since prior to demixing the system exhibits a structure reminiscent of a disordered two-phase heterogeneous material, which in this case will be shown to be hyperuniform.

The rest of the paper is organized as follows. In the next section we present our model system and provide a brief description of the theoretical and simulation methods employed, including a summary of the expressions that describe the system thermodynamics in the HNC approximation. Then, in Sec. III, we derive analytical expressions that describe the low-$Q$ behavior of our system. It will be shown that whereas the condition for global hyperuniformity is fulfilled, the systems are not multihyperuniform. Finally, in Sec. IV we present our most relevant results, with particular emphasis on the phase behavior of the NAHD plasma and how global hyperuniformity affects the concentration fluctuations that lead to demixing. The connection between hyperuniformity, "hidden order," and configurational entropy is also explored in this final section. In Sec. V, we make concluding remarks.

## II. MODEL AND METHODS

Our model consists of a symmetric mixture of nonadditive hard disks with a 2D Coulombic interaction between them, i.e., the interaction potential $u_{ij}(r)$ is given by

$$\beta u_{ij}(r) = \begin{cases} \infty & \text{if } r < [1 + \Delta(1 - \delta_{ij})]\sigma \\ -Z_i Z_j \Gamma \log r/\sigma & \text{if } r \geqslant [1 + \Delta(1 - \delta_{ij})]\sigma, \end{cases} \quad (6)$$

where $\beta = 1/k_B T$ as usual, and $\Gamma = \beta e^2$, where $e$ is the electron charge (esu units). Also, $Z_i$, is the particle charge in $e$ units (for simplicity we will just consider $Z_i = 1$), $\Delta$ is the nonadditivity parameter, and $\sigma$ the hard disk diameter between like species. Obviously, increasing $Z_i$ is completely equivalent to modifying the coupling parameter, $\Gamma$. Moreover, we restrict ourselves to the case $Z_i = Z_j$, since for Coulombic systems charge asymmetry destroys global hyperuniformity, as shown in the discussion of Eq. (39) below. Our system will be a mixture of total surface density, $\rho$. Theoretical calculations will be presented for the equimolar mixture $\rho_1 = \rho_2 = \rho/2$,

TABLE I. Thermodynamics of the equimolar NAHD plasma for $\rho\sigma^2 = 0.8$ and $\Delta = -0.2$ as computed from MC simulations and in the HNC and RHNC-PY approximations.

| | MC | RHNC-PY | HNC | | | |
|---|---|---|---|---|---|---|
| $\Gamma$ | $\beta U^{ex}/N$ | $\beta U^{ex}/N$ | $\beta U^{ex}/N$ | $\beta A^{ex}/N$ | $S^{ex}/Nk_B$ | $S_2^{ex}/Nk_B$ | $\Delta S^{ex}/Nk_B$ |
| 0.0 | 0 | 0 | 0 | 1.878 | −1.878 | −1.4520 | −0.426 |
| 0.5 | −0.248 | −0.2507 | −0.2407 | 1.651 | −1.892 | −1.4279 | −0.464 |
| 1.0 | −0.512 | −0.5168 | −0.4990 | 1.405 | −1.904 | −1.4121 | −0.492 |
| 2.0 | −1.053 | −1.0652 | −1.0318 | 0.897 | −1.929 | −1.3889 | −0.540 |
| 5.0 | −2.733 | −2.7716 | −2.6840 | −0.688 | −1.996 | −1.3456 | −0.650 |

i.e., the mole fractions will be simply $x_1 = x_2 = 1/2$. We do not expect any new physics to arise from nonequimolar compositions. One would simply find a species-dependent asymmetry in the cluster number distributions for the positive nonadditive case, and for very asymmetric compositions it would be possible to reach higher total densities without demixing. For negative nonadditivities changes will be even less visible, aside from the dominance of a particular species and correspondingly lower degree of heterocoordination. Throughout the paper density will be reduced as $\rho\sigma^2$.

### A. The integral equation approach

The Ornstein-Zernike equation for a mixture is given by [25]

$$h_{jk}(r_{12}) = \sum_l \rho_l \int d\mathbf{r}_3 c_{jl}(r_{13}) h_{lk}(r_{32}), \tag{7}$$

where $c_{ij}$ is the direct correlation function, with $\rho_l$ being the number density of species $l$. In Fourier space Eq. (7) can be cast into matrix form to yield

$$\tilde{\Gamma}(Q) = [\mathbf{I} - \tilde{\mathbf{C}}(Q)]^{-1}\tilde{\mathbf{C}}(Q)\tilde{\mathbf{C}}(Q), \tag{8}$$

where $\mathbf{I}$ is the identity matrix, the tilde denotes a 2D Fourier transformation, and

$$[\tilde{\Gamma}(Q)]_{ij} = \sqrt{\rho_i\rho_j}\,\tilde{\gamma}_{ij}(Q), \tag{9}$$

$$[\tilde{\mathbf{C}}(Q)]_{ij} = \sqrt{\rho_i\rho_j}\,\tilde{c}_{ij}(Q), \tag{10}$$

with $\gamma_{ij} \equiv h_{ij} - c_{ij}$. The closure for Eq. (7) reads

$$c_{ij}(r) = \exp[-\beta\phi_{ij}(r) + \gamma_{ij}(r) + B_{ij}(r)] - 1 - \gamma_{ij}(r), \tag{11}$$

where $B_{ij}(r)$ is the bridge function. Here we will make use of two approximations, namely, $B_{ij}(r) = 0$, i.e., the HNC approximation, and $B_{ij}(r) = B_{ij}^{\mathrm{HS-PY}}(r)$, where this latter function is the bridge function computed in the Percus-Yevick (PY) approximation for the plain NAHD system without electrostatic interactions. We will denote this approximation by RHNC-PY. These equations can now be solved by a simple iterative procedure, provided the long-range character of the correlations is appropriately treated. Following Ref. [32] we define a well-behaved long-range component of the interaction

$$\beta\phi_{ij}^{\mathrm{LR}}(r) = -Z_iZ_j\Gamma\left[\ln\left(\frac{r}{\sigma}\right) + \frac{1}{2}E_1\left(\frac{r^2}{\sigma^2}\right)\right], \tag{12}$$

$$\beta\tilde{\phi}_{ij}^{\mathrm{LR}}(Q) = Z_iZ_j\Gamma\frac{2\pi}{(k\sigma)^2}\exp\left[-\frac{1}{4}(k\sigma)^2\right], \tag{13}$$

where $E_1(x)$ is the exponential integral. With these, one can construct a set of short-range correlations and interactions of the form

$$\beta\phi_{ij}^{\mathrm{SR}}(r) = \beta\phi_{ij}(r) - \beta\phi_{ij}^{\mathrm{LR}}(r), \tag{14}$$

$$c_{ij}^{\mathrm{SR}}(r) = c_{ij}(r) - \beta\phi_{ij}^{\mathrm{LR}}(r), \tag{15}$$

$$\gamma_{ij}^{\mathrm{SR}}(r) = \gamma_{ij}(r) + \beta\phi_{ij}^{\mathrm{LR}}(r), \tag{16}$$

and similarly for their Fourier transforms. Equation (8) and its closure (11) can be solved without further complications. A more detailed description of the procedure can be found in Ref. [32] and references therein. Here the equations have been solved over 2000 grid points covering a range in $r$ space of $20\sigma$.

### B. Hypernetted Chain equation thermodynamics

In what follows, we summarize the key equations to compute the thermodynamics of our system in the HNC approximation. Our choice is based on the internal consistency of all thermodynamic properties in the HNC (with the exception of the isothermal compressibility computed from the fluctuation theorem), which can be used to test the correctness of our results. The excess internal energy is simply given by

$$\beta U^{\mathrm{ext}}/N = -\frac{1}{\rho}\sum_{\alpha,\beta} Z_\alpha Z_\beta \rho_\alpha \rho_\beta \Gamma\pi \int dr r[g_{\alpha\beta}(r) - 1]\log(r/\sigma). \tag{17}$$

The presence of the neutralizing background is apparent in the above expression through the term involving $-1$ in $g_{\alpha\beta}(r) - 1$. The accuracy of the internal energy calculation is high in the HNC, as can be appreciated in Table I. Even though the RHNC-PY provides slightly better results, here we will mostly make use of the HNC thermodynamics, since quantities such as the chemical potential and Helmholtz energy can be evaluated directly from the correlation functions, and as mentioned above, it is endowed with a high degree of thermodynamic consistency. Specifically, the Helmholtz's free energy can be evaluated as the sum of two contributions

$$\beta A^{\mathrm{ex}}/N = \beta A_1^{\mathrm{ex}}/N + \beta A_2^{\mathrm{ex}}/N, \tag{18}$$

obtained by a set of integrals in physical **r** space and $Q$ space:

$$\beta A_1^{\rm ex}/N = \frac{\pi}{\rho}\sum_{\alpha,\beta}\rho_\alpha\rho_\beta\left(-\frac{\Gamma}{4}Z_\alpha Z_\beta + \int dr r\left\{c_{\alpha,\beta}^{\rm SR}(r) + \frac{1}{2}\left[c_{\alpha,\beta}^2(r) - \gamma_{\alpha,\beta}^2(r)\right]\right\}\right),$$

$$\beta A_2^{\rm ex}/N = -\frac{1}{2\rho}\int dQ\,Q\{\log|\mathbf{I} + \tilde{\mathbf{H}}(Q)/Q^{-1}| - {\rm Tr}[\tilde{\mathbf{H}}(Q)/Q^{-1}]\}. \tag{19}$$

One can also calculate the free energy from the chemical potential in the HNC, which is given by

$$\beta\mu_i^{\rm ex} = -\sum_\alpha \rho_\alpha \tilde{c}_{i\alpha}^R(0) + \frac{\pi}{2}\sum_\alpha \rho_\alpha \int h_{i\alpha}(r)[h_{i\alpha}(r) - c_{i\alpha}(r)]r\,dr, \tag{20}$$

where

$$\tilde{c}_{ij}^R(0) = \tilde{c}_{ij}^{\rm SR}(0) + \frac{\pi}{2}\Gamma Z_i Z_j \tag{21}$$

is the $Q \to 0$ limit of the regular part of the direct correlation [28]. With this one gets

$$\beta A^{\rm ex}/N = \sum_i \rho_i \beta\mu^{\rm ex} - \beta P/\rho + 1. \tag{22}$$

The pressure can be computed from the virial equation, that in the case of the NAHD two-component plasma is simply

$$\beta P/\rho = 1 + \frac{1}{4\rho}\pi\sum_{\alpha,\beta}\rho_\alpha\rho_\beta\sigma_\alpha\sigma_\beta g_{\alpha\beta}(\sigma_{\alpha\beta}^+) - \frac{1}{4}\Gamma. \tag{23}$$

The fact that the Coulomb contribution equals $-\Gamma/4$ can be used as an internal consistency check of the results by numerically integrating the correlation functions with the corresponding virial factors.

From these expressions, the excess configurational entropy is obtained as

$$S^{\rm ex}/Nk_B = \beta U^{\rm ex}/N - \beta A^{\rm ex}/N. \tag{24}$$

Additionally, one can determine the two-particle excess configurational entropy contribution layer by layer using

$$S_2^{\rm ex}(R)/Nk_B = -\pi\rho\sum_{\alpha,\beta}x_\alpha x_\beta\int_0^R [g_{\alpha\beta}(r)\log g_{\alpha\beta}(r) - g_{\alpha\beta}(r) + 1]r\,dr. \tag{25}$$

The total two-particle contribution corresponds to $S_2^{\rm ex}(\infty)/Nk_B$. This quantity accounts in most cases for more than 80% of the total configurational entropy [33]. We will see later that our case deviates from the standard behavior in regular fluids. A relevant quantity in connection with the configurational entropy, $S^{\rm ex}$ and its two-particle contribution, $S_2^{\rm ex}$, is their difference $\Delta S^{\rm ex}/Nk_B = S^{\rm ex}/Nk_B - S_2^{\rm ex}/Nk_B$. For purely repulsive interactions, the presence of zeros in $\Delta S^{\rm ex}(\rho)/Nk_B$ has been correlated with the location of a fluid-solid transition [33]. Finally, it is worth mentioning that the two-particle excess entropy is closely related with the $\tau$-order metrics parameter, which is a measure of translational order [2],

$$\tau = \frac{\pi\rho}{D}\sum_{\alpha,\beta}x_\alpha x_\beta\int h_{\alpha\beta}(r)^2 r\,dr = \frac{1}{D}\sum_{\alpha,\beta}\int[S_{\alpha\beta}(\mathbf{Q}) - x_\alpha\delta_{\alpha\beta}][S_{\alpha\beta}(-\mathbf{Q}) - x_\alpha\delta_{\alpha\beta}]d\mathbf{Q}, \tag{26}$$

where $D$ is a suitable characteristic length (e.g., correlation length). This expression is in fact the multicomponent generalization of the $\tau$ order metric defined in Ref. [2]. Importantly, the $\tau$ order parameter defined by (26) is given in terms of quantities that are experimentally accessible. Note that a closely related order metric was defined in physical space in terms of $|h(r)|$ [34], instead of $h(r)^2$. Obviously, while this does not modify the qualitative behavior of the order parameter, it does not have a corresponding representation in terms of the structure factor. Comparing Eqs. (25) and (26), one sees that the latter can easily be obtained from (25) by a small $h$ expansion of the integrand, with the sign changed. Ordered systems (e.g., crystals) will give infinite $\tau$, whereas for the ideal gas $\tau$ vanishes, as the does the excess two-particle entropy.

### C. Details of the simulation procedure

The MC simulations were performed mostly in the canonical ensemble using $N$ particles embedded in a uniform neutralizing background in a square box of side $L$ with periodic boundary conditions. The energy of the periodic system was evaluated by the Ewald summation method with conducting boundary conditions [35]:

$$\begin{aligned}\beta U^{\rm ex} = {}& \frac{\Gamma}{4}\sum_{i=1}^N\sum_{j=1}^N Z_i Z_j {\sum_{\mathbf{n}}}' E_1\left(\alpha*^2\left|\frac{\mathbf{r}_{ij}}{L} + \mathbf{n}\right|\right) \\ & + \frac{\Gamma}{4\pi}\sum_{\mathbf{n}\neq 0}\frac{e^{-\pi^2\mathbf{n}^2/\alpha*^2}}{\mathbf{n}^2}\left|\sum_{i=1}^N Z_i\exp\left(2\pi i\mathbf{n}\cdot\frac{\mathbf{r}_i}{L}\right)\right|^2 \\ & - \frac{\Gamma}{4}(\gamma + \ln\alpha*^2)\sum_{i=1}^N Z_i^2 + \frac{\Gamma\pi}{4\alpha*^2}\sum_{i=1}^N Z_i^2 \\ & + \frac{\Gamma}{2}\ln\left(\frac{L}{\sigma}\right)\sum_{i=1}^N Z_i^2.\end{aligned} \tag{27}$$

In Eq. (27), $\mathbf{r}_{ij} = \mathbf{r}_j - \mathbf{r}_i$, and $\gamma = 0.5772156\ldots$ is Euler's constant. The prime in the sum over $\mathbf{n} = (n_x, n_y)$, with $n_x, n_y$ integers, restricts it to $i \neq j$ for $\mathbf{n} = 0$. The dimensionless parameter $\alpha^* = \alpha L$ controls the relative contributions to the Ewald sum of the direct and reciprocal space terms. With the choice $\alpha^* = 6$, adopted in our calculations, only terms with $\mathbf{n} = 0$ need to be retained in the first sum of Eq. (27). The sum in reciprocal space extends over all lattice vectors $\mathbf{k} = 2\pi\mathbf{n}/L$ with $|\mathbf{n}^2| \leqslant 64$. The fourth term in Eq. (27) represents the interaction of the background with itself. In the simulations the Coulomb potential was scaled by $L$ rather than $\sigma$ as in the theoretical approaches. The last term in Eq. (27) was added to meet the theoretical choice.

We note here that in Ref. [29] periodic boundary conditions and Ewald sums are not required, since the system is simulated on the surface of a sphere. In principle, both methods should lead to similar results, particularly for relatively large samples, like those used in this work. But on the other hand, a key quantity in our calculation is the structure factor, and one can easily appreciate that its determination on a spherical surface is substantially more cumbersome than on a plane. These considerations have led us to employ the simulation procedure sketched above.

In the vicinity of the demixing transition which occurs for positive nonadditivity of the disks we performed semigrand canonical MC simulations along the lines detailed in Ref. [31] for the plain NAHD system. In particular, we took advantage of the cluster algorithm described in Ref. [31] for identity sampling. Two particles of the same species are considered linked within the same cluster when their separation is less than $\sigma(1 + \Delta)$. With this choice cluster identity swaps do not lead to particle overlaps, and for the present symmetrical case where the chemical potential difference $\Delta\mu = \mu_A - \mu_B = 0$, the procedure leads to a rejection-free algorithm of composition sampling for a fixed set of particle positions [31].

Most simulations used 1600, 2500, and 3600 particles, and generally structural properties or order parameters were obtained by averaging over $3 \times 10^6$ to $5 \times 10^6$ trial translational moves per particle after equilibration of the system. An identity swap was performed after five translational moves. Further calculations were carried out with 6100 and 8400 particles to allow for a more precise determination of the consolute point of the mixture. The effects of system size on the structural properties are practically negligible for all our samples. The dependence of the Binder's cumulants on the sample size is used to determine the critical demixing density [36] [see Eq. (40) and the discussion below].

## III. LOW-$Q$ BEHAVIOR

Starting from the matrix form of the Ornstein-Zernike equation (7)

$$\mathbf{I} + \mathbf{H} = [\mathbf{I} - \mathbf{C}]^{-1}, \tag{28}$$

one gets explicitly for the components of the partial structure factors (3)

$$1 + \rho_i \tilde{h}_{ii} = \frac{1 - \rho_j \tilde{c}_{jj}}{|\mathbf{I} - \mathbf{C}|}, \tag{29}$$

$$\sqrt{\rho_i \rho_j}\tilde{h}_{ij} = \frac{\sqrt{\rho_i \rho_j}\tilde{c}_{ij}}{|\mathbf{I} - \mathbf{C}|}, \tag{30}$$

with $i \neq j$ and

$$|\mathbf{I} - \mathbf{C}| = 1 - \rho_1\tilde{c}_{11} - \rho_2\tilde{c}_{22} + \rho_1\rho_2\big(\tilde{c}_{11}\tilde{c}_{22} - \tilde{c}_{12}^2\big). \tag{31}$$

The situation simplifies for the symmetric system, $c_{11} = c_{22}$, $\rho_1 = \rho_2 = \rho/2$. One can perform a small-$Q$ expansion of the direct correlation function separating the Coulomb term:

$$\tilde{c}_{ij}(Q) \approx \tilde{c}_{ij}^R(0) + c_{ij}^{(2)}Q^2 - 2\pi\Gamma Z_i Z_j/Q^2. \tag{32}$$

The expansion coefficients of $\tilde{c}_{ij}^R(Q)$ are simply given by

$$c_{ij}^{(2)} = \frac{1}{2}\left.\frac{\partial\tilde{c}_{ij}^R(Q)}{\partial Q}\right|_{Q=0}. \tag{33}$$

These $Q^2$ contributions are needed to reproduce the low-$Q$ behavior of the partial structure factors beyond $Q = 0$.

Using the expressions above, one can obtain the following limiting behavior:

$$1 + \rho_1\tilde{h}_{11}(Q) \approx \frac{\big\{1 - \frac{\rho}{2}\big[\tilde{c}_{11}^R(0) + c_{11}^{(2)}Q^2\big]\big\}Q^2 + \pi\rho\Gamma Z^2}{(aQ^2 + 2\pi\rho\Gamma Z^2)b},$$

$$\rho\sqrt{x_1x_2}\tilde{h}_{12}(Q) \approx \frac{\frac{\rho}{2}\big[\tilde{c}_{12}^R(0) + c_{11}^{(2)}Q^2\big]Q^2 - \pi\rho\Gamma Z^2}{(aQ^2 + 2\pi\rho\Gamma Z^2)b}, \tag{34}$$

when $Q \to 0$, with

$$a = 1 - \tfrac{\rho}{2}\big[\tilde{c}_{11}^R(0) + \tilde{c}_{12}^R(0) + \big(c_{11}^{(2)} + c_{12}^{(2)}\big)Q^2\big],$$

$$b = 1 - \tfrac{\rho}{2}\big[\tilde{c}_{11}^R(0) - \tilde{c}_{12}^R(0) + \big(c_{11}^{(2)} - c_{12}^{(2)}\big)Q^2\big].$$

For the total structure factor, in our fully symmetric mixture we have

$$S_{\mathrm{NN}}(Q) = 2S_{11}(Q) + 2S_{12}(Q) \tag{35}$$

by which

$$S_{\mathrm{NN}}(Q) \approx \frac{Q^2}{aQ^2 + 2\pi\rho\Gamma Z^2}. \tag{36}$$

This differs slightly from the pure one-component plasma (OCP) behavior [29] for which $a = 1$, since core contributions vanish. In our case non-negligible contributions from the hard core become more evident as $Q$ grows.

For the concentration-concentration structure factor we have

$$S_{\mathrm{cc}}(Q) = \tfrac{1}{2}[S_{11}(Q) - S_{12}(Q)], \tag{37}$$

which leads to

$$S_{\mathrm{cc}}(Q) \approx \frac{1}{4b} = \frac{1}{4\big\{1 - \frac{\rho}{2}\big[\tilde{c}_{11}^R(0) - \tilde{c}_{12}^R(0) + \big(c_{11}^{(2)} - c_{12}^{(2)}\big)Q^2\big]\big\}}$$

$$= \frac{1}{4 + s + tQ^2}, \tag{38}$$

where the constants $s$ and $t$ depend on density and on the short-range behavior of the direct correlation functions.

From the expressions (34), it is clear that

$$\lim_{Q\to 0}[1 + \rho_1\tilde{h}_{11}(Q)] = \frac{1}{2\big\{1 - \frac{\rho}{2}\big[\tilde{c}_{11}^R(0) - \tilde{c}_{12}^R(0)\big]\big\}},$$

$$\lim_{Q\to 0}[\rho\sqrt{x_1x_2}\tilde{h}_{11}(Q)] = -\frac{1}{2\big\{1 - \frac{\rho}{2}\big[\tilde{c}_{11}^R(0) - \tilde{c}_{12}^R(0)\big]\big\}},$$

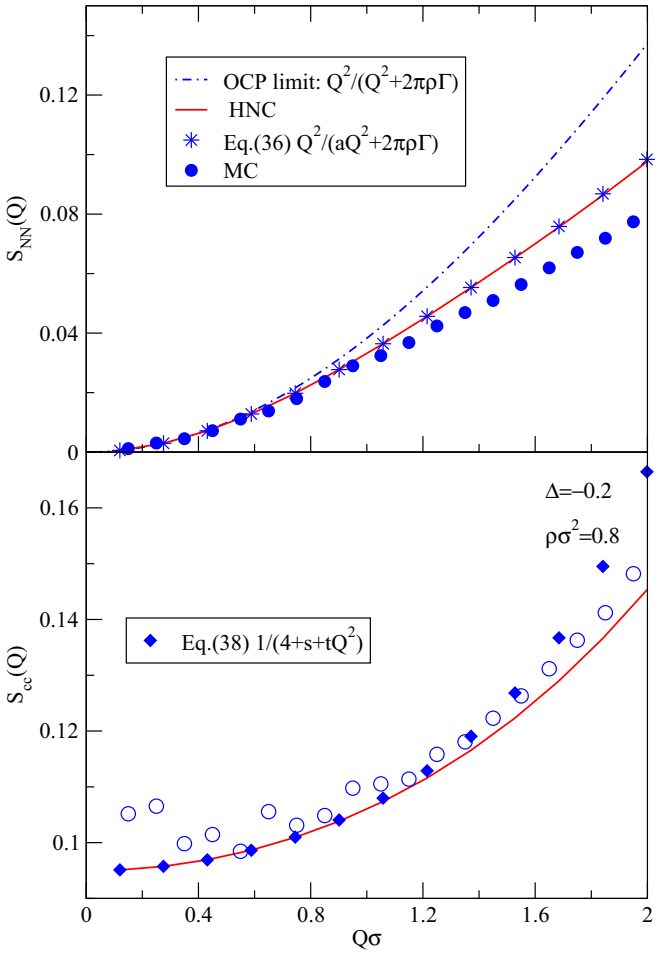


FIG. 1. Low-$Q$ behavior of the $S_{NN}$ and $S_{cc}$ structure factors for an equimolar hard disk plasma mixture with negative nonadditivity, as determined by simulation and in the HNC approximation. The low-$Q$ HNC expansion from Eq. (36) and the pure OCP limit ($a = 1$) are also illustrated for $S_{NN}(Q)$, together with the limiting formula (38) for $S_{cc}(Q)$. Diamonds and stars represent these limiting analytic expressions to ease the comparison with the HNC results (solid lines). Filled and open circles denote simulation results.

which shows definitely that the system is not multihyperuniform, although globally it has a hyperuniform behavior given by Eq. (36), i.e., $S_{NN}(Q) \propto Q^2$ ($Q \to 0$). In Fig. 1 the validity of expressions (36) and (38) is illustrated for a NAHD plasma with negative nonadditivity. For comparison the OCP limiting behavior is also shown and can be seen to deviate already at $Q\sigma \sim 0.6$. At this point is it important to stress that the global hyperuniformity summarized in Eq. (36) is the result of the symmetry relation

$$\lim_{Q\to 0} [\tilde{u}_{11}(Q) + \tilde{u}_{22}(Q) - 2\tilde{u}_{12}(Q)] = 0 \qquad (39)$$

being fulfilled by the long-range contributions to the interactions. Obviously, repulsive Coulomb systems comply with Eq. (39) whenever $Z_1 = Z_2$.

## IV. RESULTS

We have first focused our investigations in a case of positive nonadditivity, $\Delta = 0.2$, whose phase behavior has already been studied in detail for the uncharged system [31]. This NAHD mixture is known to exhibit a demixing transition with Ising 2D criticality. Additionally, we have also considered the situation with negative nonadditivity, $\Delta = -0.2$, which is characterized by the absence of a demixing transition and a tendency to present local heterocoordination.

TABLE II. Thermodynamics of the equimolar NAHD plasma for $\rho\sigma^2 = 0.6$ and $\Delta = 0.2$ computed in the HNC approximation.

| $\Gamma$ | $\beta U^{ex}/N$ | $\beta A^{ex}/N$ | $S^{ex}/Nk_B$ | $S_2^{ex}/Nk_B$ | $\Delta S^{ex}/Nk_B$ |
|---|---|---|---|---|---|
| 0.0 | 0 | 2.301 | −2.301 | −1.9947 | −0.306 |
| 0.5 | −0.2140 | 2.097 | −2.311 | −1.9484 | −0.362 |
| 1.0 | −0.4423 | 1.879 | −2.321 | −1.9210 | −0.400 |
| 2.0 | −0.9125 | 1.429 | −2.342 | −1.8813 | −0.461 |
| 5.0 | −2.3677 | 0.030 | −2.398 | −1.8054 | −0.593 |

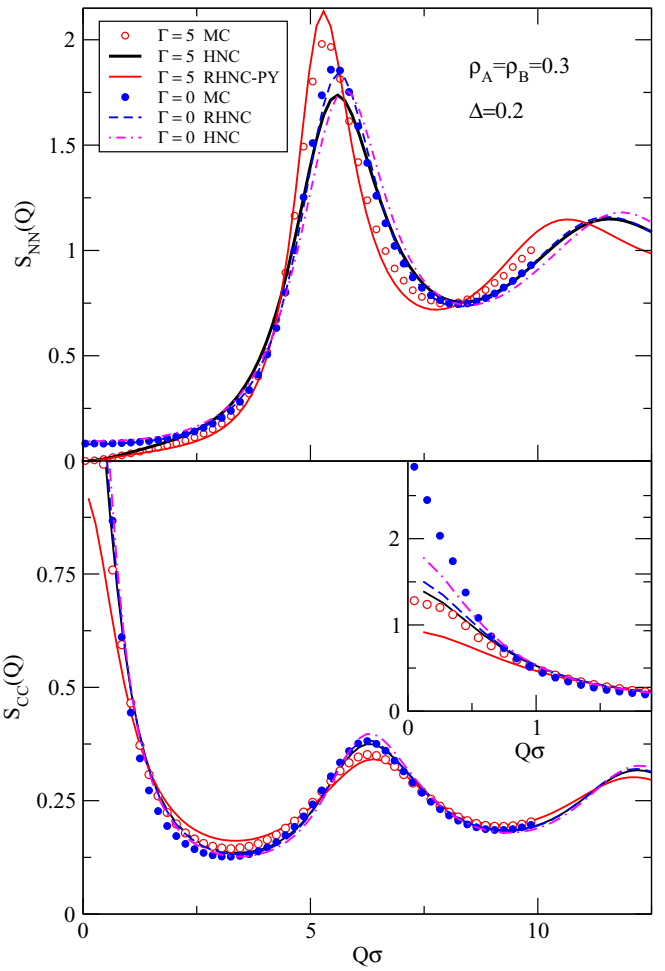


FIG. 2. Density-density, $S_{NN}$, and concentration-concentration, $S_{cc}$, structure factors for the equimolar NAHD plasma ($\Gamma = 5$) and plain NAHD system $\Gamma = 0$ for positive nonadditivity. Curves denote various theoretical approaches (shown on the legend) and symbols MC data. The effect of global hyperuniformity is seen for the charged system, as $\lim_{Q\to 0} S_{NN}(Q) = 0$.

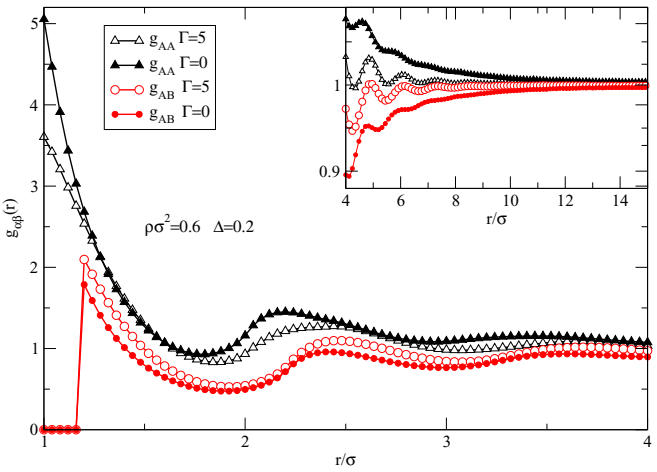


FIG. 3. Pair distribution functions for the equimolar NAHD plasma ($\Gamma = 5$) and plain NAHD system $\Gamma = 0$ for positive nonadditivity as obtained from MC simulation. The inset illustrates the long-range behavior. Long-range correlations are damped by the presence of charges, as an effect of global hyperuniformity.

### A. Positive nonadditivity and demixing transition

In Ref. [31], it was found that the uncharged system exhibits a phase separation when $\Delta = 0.2$ with a consolute point at $\rho_c\sigma^2 = 0.69$ (and obviously $x_1 = x_2 = 1/2$). We have first studied the system at a somewhat lower total density, $\rho\sigma^2 = 0.60$, and a relatively large Coulombic coupling, $\Gamma = 5$. Thermodynamic properties for this system in the HNC approximation are collected in Table II.

The effect of the charges is readily seen in the density-density correlations represented by the total structure factor (see Fig. 2), which now vanishes as $Q \to 0$, making the system globally hyperuniform. On the other hand, in the lower graph of Fig. 2 for $S_{cc}(Q)$ we can observe that there are large concentration fluctuations when $Q \to 0$, i.e., for large separations. This is a clear indication of the vicinity of the demixing transition. Interestingly, one observes that $S_{cc}(0)(\Gamma = 5) < S_{cc}(0)(\Gamma = 0)$, i.e., charges (or global hyperuniformity) counteract to a certain extent the tendency to demix. This effect is further illustrated by the long-range behavior of the pair distributions depicted in Fig. 3. One readily observes that the long-range oscillations of like and unlike $g_{\alpha\beta}$ in the uncharged system (an indication of the approaching divergence at the critical density) are quite damped due to the effect of the charges. Overall, one sees that the values of the like correlations at short and intermediate ranges are lowered when charges are introduced, which reflects the repulsive nature of the Coulomb interaction in the plasma. In contrast, unlike correlations grow, since the Coulombic repulsion has a larger effect on like particles whose distance of closest approach is $\sigma$, which is lower than $(1 + \Delta)\sigma$, for unlike particles. One can easily see in the snapshots of Fig. 4 that this translates into a situation for which the size of the clusters of like particles decreases when charges are present. Here we have one of these situations in which global hyperuniformity leads to some sort of long-range "hidden" order invisible to the eye. In contrast, the effect on the compositional order is readily appreciated.

As to the net effect on the phase behavior, in Fig. 5 we present the phase diagram for the plain NAHD system, taken from Ref. [31] and that obtained in this work for $\Gamma = 5$.

The critical point estimates are calculated from the crossings of Binder's cumulants [36], $U_4$ and $U_6$,

$$U_{2n} = \frac{\langle\theta^{2n}\rangle}{\langle\theta^2\rangle^n}, \tag{40}$$

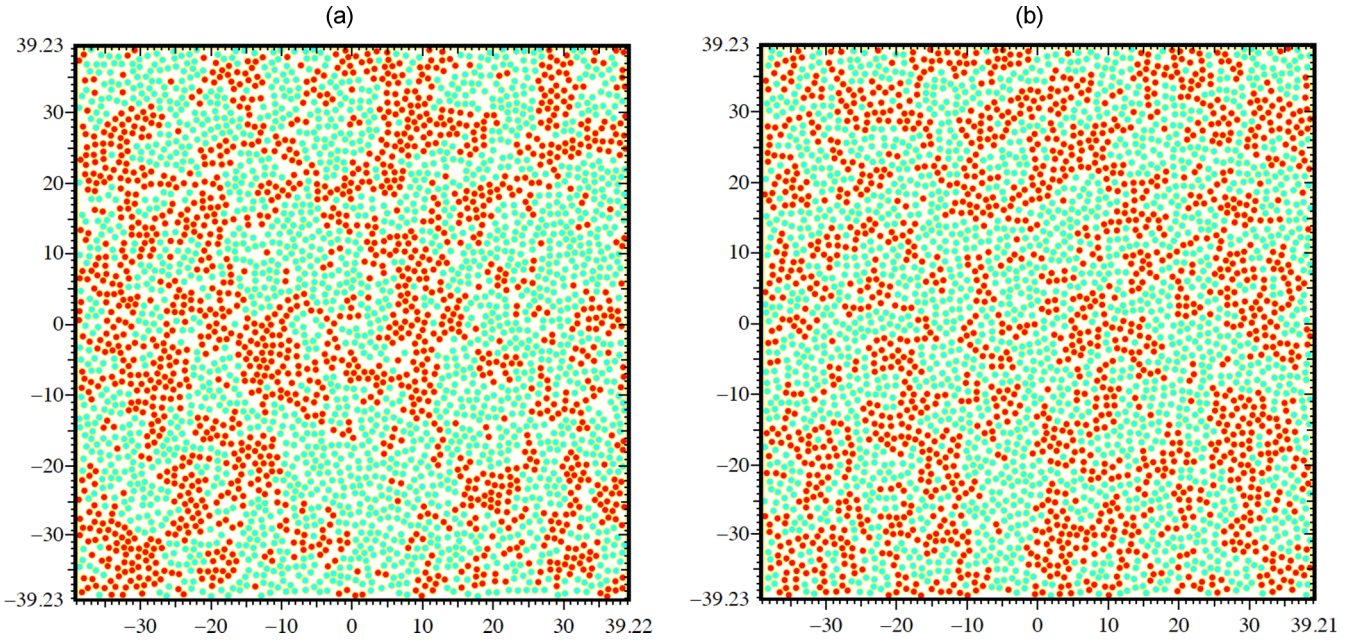


FIG. 4. Snapshots of MC configurations of the equimolar plain NAHD system (a) $\Gamma = 0$ and the NAHD two-component plasma for $\Gamma = 5$ (b) and positive nonadditivity, $\Delta = 0.2$, for $\rho\sigma^2 = 0.6$. The effect of global hyperuniformity cannot be appreciated on the translational order, but on the compositional order it can be seen that the presence of charges tends to reduce the size of the clusters.

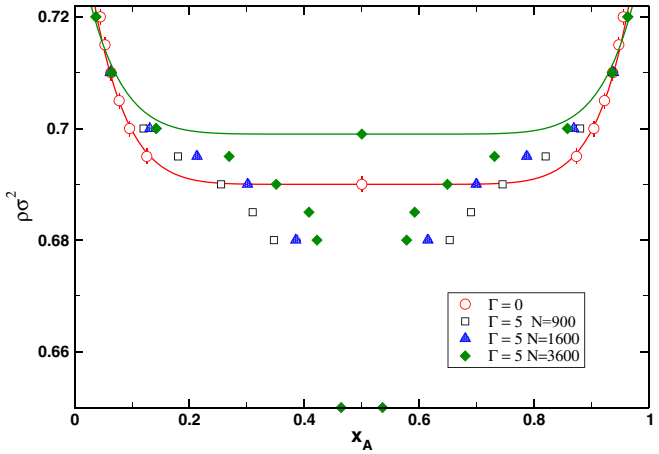


FIG. 5. Phase diagram of the NAHD system and the NAHD plasma with $\Gamma = 5$. Symbols correspond to semigrand ensemble simulations for different system sizes. The critical point estimates are obtained from the crossing of Binder's $U_{2n}$ cumulants [see Eq. (40)], and the lines are a fit to Ising 2D critical behavior.

where the $\langle \ldots \rangle$ denotes an ensemble average, and $\theta = 2x - 1$. The size dependence of these quantities is illustrated in Fig. 6, from which one can estimate the critical density determined by the crossing of the curves. One obtains $\rho_c\sigma^2 \approx 0.699$, slightly larger than the value for the plain NAHD system, $\rho_c\sigma^2 \approx 0.69$. This agrees with our previous findings that indicated that global hyperuniformity, damping long-range correlations, tends to counteract phase separation. Still, short-range volume effects cannot be completely canceled out by the subtle changes induced by global hyperuniformity, and the system demixes at a higher density. As to the crossing of the cumulants, for $U_4$, one gets $U_4^c \approx 1.15 \pm 0.02$, which means that the accepted Ising 2D universal value [37], $U_4^c \approx 1.168$, lies within the uncertainty of our calculation. Here then, for our purposes, we have assumed 2D Ising criticality [37], and thus the fitted curves of Fig. 5 are obtained using a critical exponent $\beta = 1/8$.

### B. Negative nonadditivity: Heterocoordination

Thermodynamic properties for the NAHD system with $\rho\sigma^2 = 0.8$ and $\Delta = -0.2$ are collected in Table I for various couplings. As to the structure, in the snapshots of Fig. 7 one can qualitatively appreciate the effects of the charges (i.e., global hyperuniformity) on the microscopic structure of the fluid. On the left (uncharged NAHD) one can see that system tends to heterocoordination, maximizing the contacts between unlike particles and thus minimizing volume. Switching on the Coulombic repulsion, even though it affects all particles in the same degree, has more apparent effects for pairs of unlike particles. In this case, their hard core repulsion allows for closer contact, and as a consequence, heterocoordination is no longer so favorable. One can then appreciate a slight increase of like particle "aggregates." As a matter of fact, this is quantitatively illustrated by the behavior of the partial pair distribution functions depicted in Fig. 8. There one can appreciate the considerable drop in the contact value of the unlike pair distribution function (in contrast with the situation

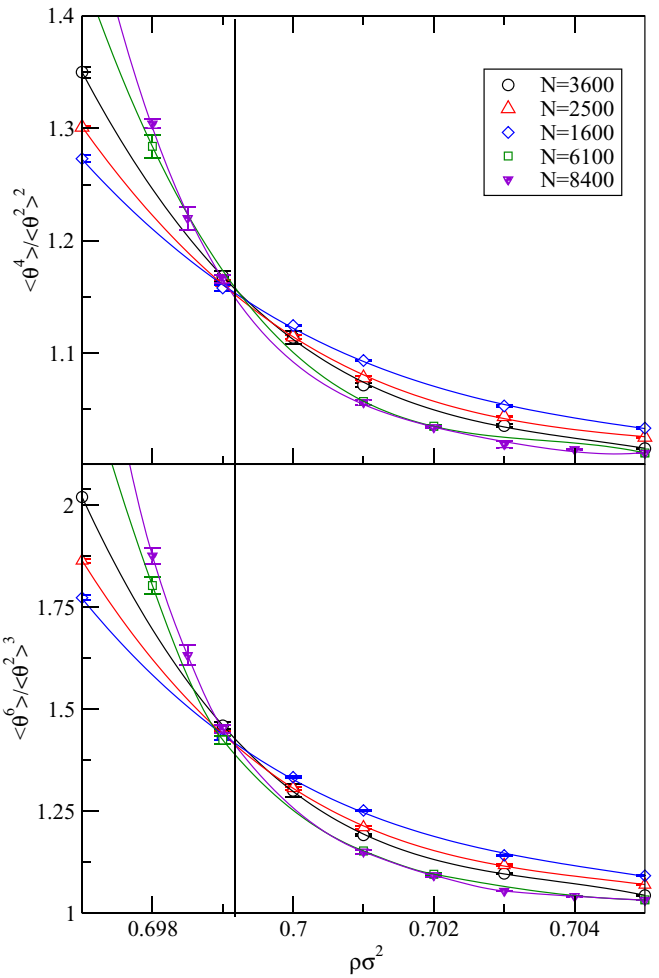


FIG. 6. Size dependence of Binder's $U_4$ and $U_6$ cumulants as a function of total density. The crossing for all curves is indicated by a vertical line and is seen to occur in the same density, $\rho_c\sigma^2 \approx 0.699$.

for positive nonadditivity seen in Fig. 3). Moreover, the like distribution function also decreases somewhat, although to a much lesser extent. For this reason, the snapshot of Fig. 7(b) seems to present a certain degree of clustering of like particles. This feature translates into a total structure factor that decays to zero following (36) (i.e., a globally hyperuniform system), and a concentration-concentration structure factor with a low-$Q$ behavior given by Eq. (38), as discussed in Sec. III and illustrated in Fig. 1. Additionally, in Fig. 9, we observe long-range oscillations in $S_{cc}(Q)$ (with a period of $Q_l \approx 7\sigma^{-1}$) that actually reflect the presence of heterocoordination (i.e., changes in local concentration over a range $2\pi/Q_l \approx 0.9\sigma \approx \sigma_{\alpha\beta}$). The presence of charges somewhat damps the oscillations, i.e., it counteracts the heterocoordination induced by volume effects.

### C. Entropy and hyperuniformity

As mentioned before, the two-particle contribution to the configurational entropy (25) usually accounts for 80% of the total configurational entropy. One can actually estimate the different contributions of each particle layer from $S_2^{ex}(R)/Nk_B$ and thus analyze the effect of charges on disorder (or more

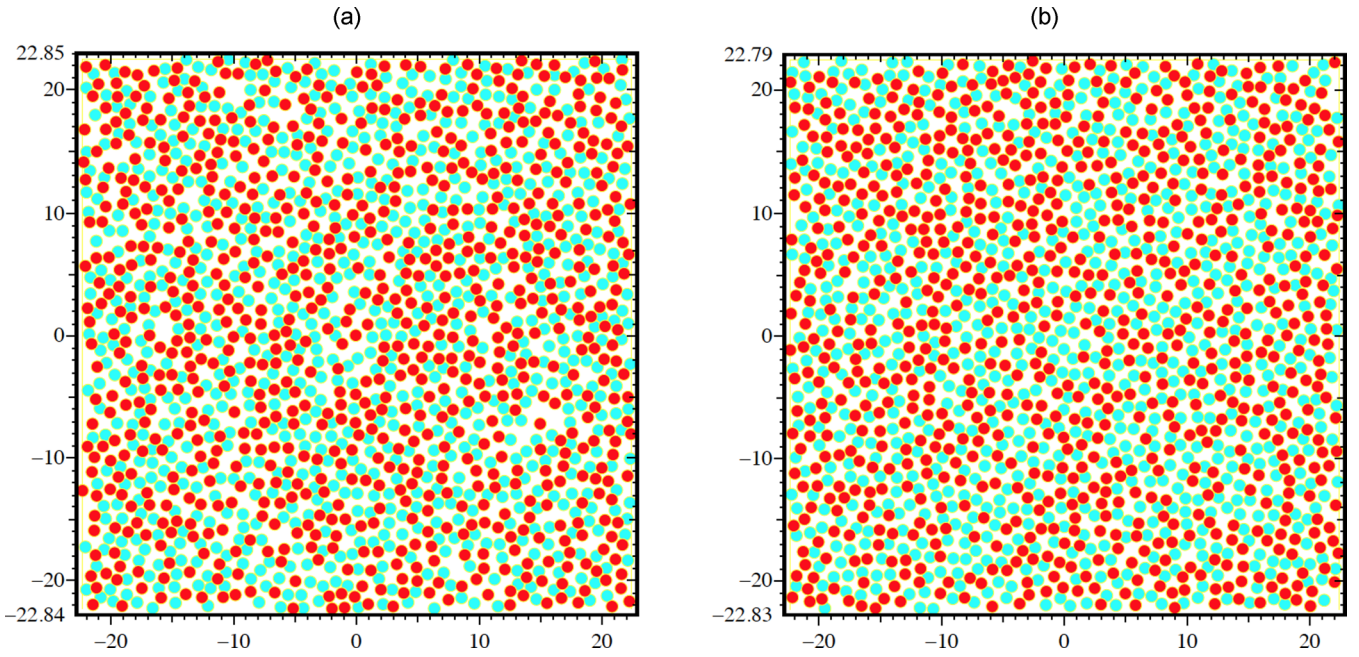


FIG. 7. Snapshots of MC configurations of the equimolar plain NAHD system (a) $\Gamma = 0$ and the NAHD two-component plasma for $\Gamma = 5$ (b) and negative nonadditivity, $\Delta = -0.2$ for $\rho\sigma^2 = 0.6$. The system tends to heterocoordination, but the net Coulombic repulsion somewhat enhances clustering of like particles.

properly, on the number of configuration/microstates compatible with our thermodynamic state). In Fig. 10 we have plotted this quantity for both the positive and negative nonadditivity computed in the HNC approximation. Additionally, in the lower graph we have included the results for an additive system ($\Delta = 0$), where no volume effects are at play. In this latter instance, we chose a density that gives a hard core contribution to the pressure similar to that of the $\Delta = -0.2$ case. One should expect to find an obvious effect on the two-particle entropy due to the "hidden order" introduced by hyperuniformity. We observe that except in the uncharged system close to demixing, the two-particle excess entropy

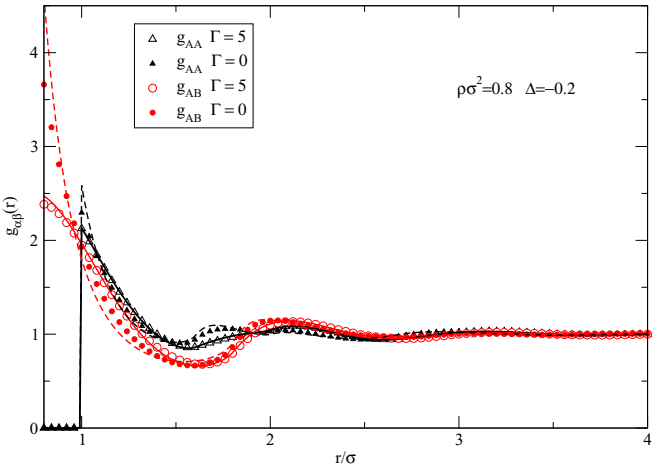


FIG. 8. Pair distribution functions for the equimolar NAHD plasma, $\Gamma = 5$, and plain NAHD system, $\Gamma = 0$, for negative nonadditivity as obtained from MC simulation (symbols) and RHNC-PY approximation (curves).

contributions originate in the first two coordination shells. For $\Gamma = 0$ and $\Delta = 0.2$ this extends up to four or five layers. Interestingly, in all instances one observes that the two-particle entropy decreases when charges are introduced (i.e., when the system becomes hyperuniform). In the case of positive nonadditivity the effect is rather extreme. As mentioned, the effect of hyperuniformity in this system counteracts phase separation. Since the system loses entropy when demixing, it is understandable that the charged system, further away from the transition, might have a larger entropy. This would explain why the two-particle contribution is less negative when charges are added. The situation is less obvious for $\Delta = 0$ and $\Delta = -0.2$. Actually, as discussed above, in Fig. 8 one already sees that the net effect of the Coulomb repulsion is a decrease in the contact values of the pair distribution functions (much more visible in the unlike case). This could be considered formally equivalent to the effect of a density decrease, which obviously would imply an increase of entropy. This scenario applies to both the positive and negative nonadditive hard disk plasmas. At least, that is the situation as far as the two-particle contribution is concerned. Note that as discussed in Sec. II B, these arguments also apply to the evolution of the translational order parameter, which is basically the negative of the two-particle entropy.

Turning attention to the net configurational entropy, Tables I and II interestingly show that the increase in entropy due to the two-particle configurational entropy is overcompensated by many-particle contributions that are approximated by the various terms that enter Eqs. (19)–(23). One can vividly see a clear decrease of the net configurational entropy. When comparing $S^{\rm ex}/Nk_B$ and $S_2^{\rm ex}/Nk_B$, it is readily seen how the relative contribution of the two-particle excess configurational entropy decreases as the system is charged, going from 80% to 67%. This is in marked contrast with the situation for "ordinary" fluids where the two-particle contribution is known

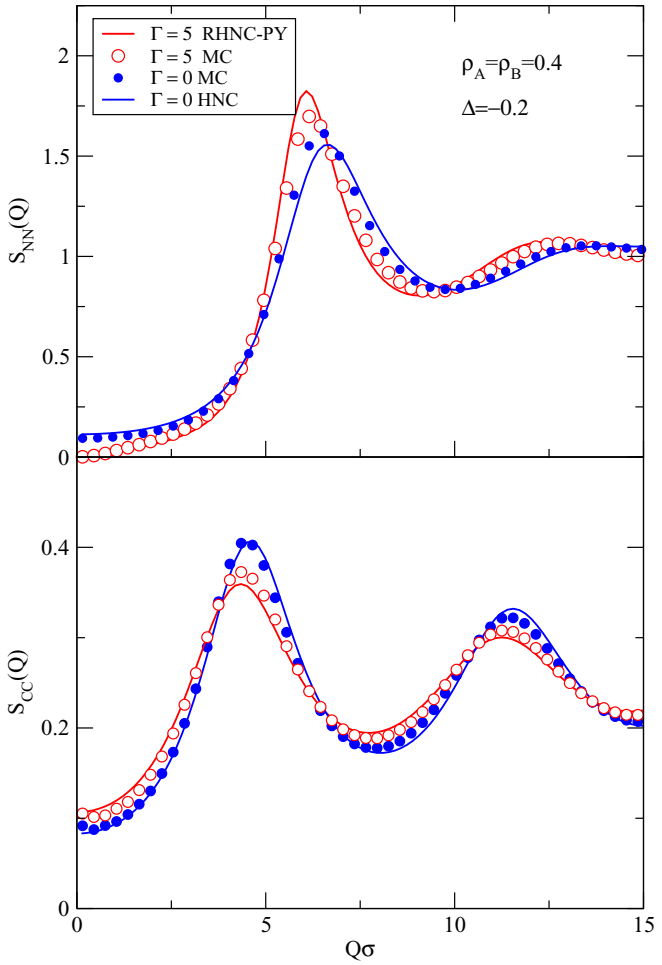


FIG. 9. Density-density, $S_{\rm NN}$, and concentration-concentration, $S_{\rm cc}$, structure factors for the equimolar NAHD plasma ($\Gamma = 5$) and plain NAHD system $\Gamma = 0$ for negative nonadditivity. Curves denote various theoretical approaches (shown on the legend) and symbols MC data. Again, the effect of global hyperuniformity is seen for the charged system, as $\lim_{Q\to 0} S_{\rm NN}(Q) = 0$.

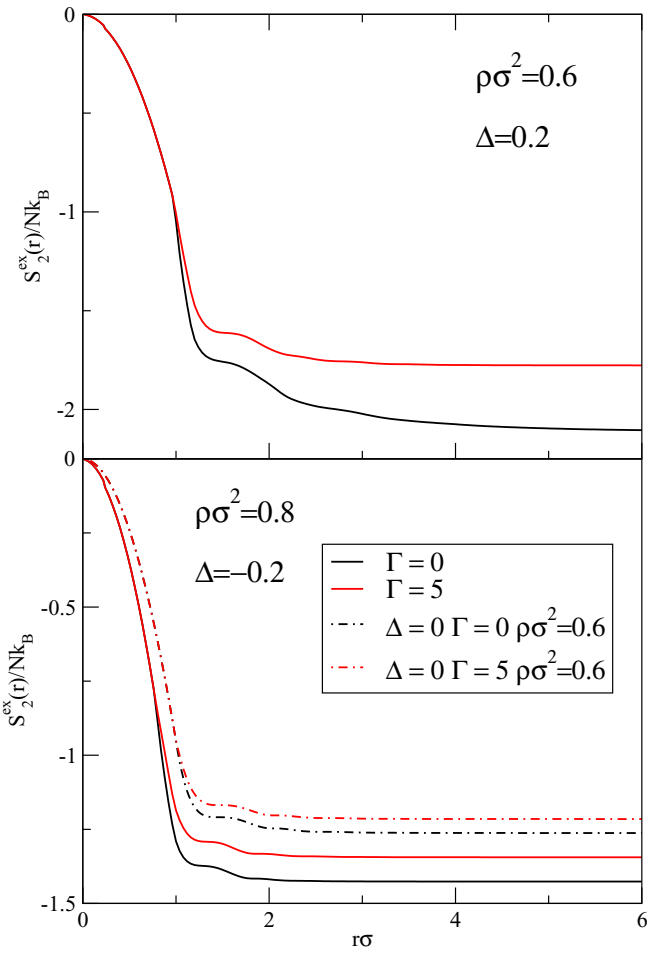


FIG. 10. Two-particle contribution to the excess configurational entropy determined in the HNC approximation for equimolar NAHD fluids, with (black curves) and without (red curves). Dash-dotted curves correspond to an additive hard sphere system with $\rho\sigma^2 = 0.6$, which gives a hard core contribution to the pressure similar to $\rho\sigma^2 = 0.8$ with $\Delta = -0.2$.

to account for 80%–90% of the total configurational entropy [33]. This reflects how the "hidden order" introduced by hyperuniformity, being a long-range effect, must influence entropy through many particle contributions: As we have seen, the two-particle configurational entropy is determined basically by the first four coordination shells.

## V. CONCLUDING REMARKS

In summary, we have shown that a simple system of NAHD with superimposed repulsive 2D Coulomb interactions can exhibit a rich structural behavior due to the interplay between the short-range volume effects leading to phase separation, clustering or heterocoordination, and the long-range effects introduced by the Coulomb forces inducing global hyperuniformity. Subtle effects are particularly visible when hyperuniformity counteracts demixing.

Finally, we note that elsewhere we have shown that by tuning interactions in binary mixtures of nonadditive hard-disk plasmas one can achieve disordered multihyperuniform many-body systems [23]. It is shown there that if $\tilde{u}_{ii}(Q) \propto Q^{-\alpha}$ for vanishing $Q$, the system will be multihyperuniform as long as $\tilde{u}_{11}(Q)\tilde{u}_{22}(Q) - \tilde{u}_{12}(Q)^2 \neq 0$. If the equality holds instead, the system will only by globally hyperuniform, provided Eq. (39) is satisfied. In Ref. [23], we also demonstrated that multihyperuniformity competes with phase separation and stabilizes a clustered phase.

## ACKNOWLEDGMENTS

Prof. Giancarlo Franzese is gratefully acknowledged for suggesting the analysis of the entropy contributions. E.L. acknowledges the support from the Dirección General de Investigación Científica y Técnica under Grant No. FIS2013-47350-C5-4-R and from the Program Salvador de Madariaga, PRX16/00069, which supports his sabbatical stay at the Chemistry Department of Princeton University. S.T. was supported by the National Science Foundation under Award No. DMR-1714722.

[1] S. Torquato and F. H. Stillinger, Phys. Rev. E **68**, 041113 (2003).
[2] S. Torquato, G. Zhang, and F. H. Stillinger, Phys. Rev. X **5**, 021020 (2015).
[3] A. Donev, F. H. Stillinger, and S. Torquato, Phys. Rev. Lett. **95**, 090604 (2005).
[4] O. U. Uche, F. H. Stillinger, and S. Torquato, Phys. Rev. E **70**, 046122 (2004).
[5] G. Zhang, F. H. Stillinger, and S. Torquato, Soft Matter **13**, 6197 (2017).
[6] G. Zhang, F. H. Stillinger, and S. Torquato, Phys. Rev. E **96**, 042146 (2017).
[7] D. Hexner and D. Levine, Phys. Rev. Lett. **114**, 110602 (2015).
[8] J. H. Weijs, R. Jeanneret, R. Dreyfus, and D. Bartolo, Phys. Rev. Lett. **115**, 108301 (2015).
[9] E. Tjhung and L. Berthier, Phys. Rev. Lett. **114**, 148301 (2015).
[10] I. Lesanovsky and J. P. Garrahan, Phys. Rev. A **90**, 011603 (2014).
[11] M. Florescu, S. Torquato, and P. J. Steinhardt, Proc. Nat. Acad. Sci. USA **106**, 20658 (2009).
[12] W. Man, M. Florescu, E. P. Williamson, Y. He, S. R. Hashemizad, B. Y. C. Leung, D. R. Liner, S. Torquato, P. M. Chaikin, and P. J. Steinhardt, Proc. Nat. Acad. Sci. USA **110**, 15886 (2013).
[13] L. S. Froufe-Pérez, M. Engel, J. José Sáenz, and F. Scheffold, Proc. Nat. Acad. Sci. USA **114**, 9570 (2017).
[14] O. Leseur, R. Pierrat, and R. Carminati, Optica **3**, 763 (2016).
[15] Y. Jiao, T. Lau, H. Hatzikirou, M. Meyer-Hermann, J. C. Corbo, and S. Torquato, Phys. Rev. E **89**, 022721 (2014).
[16] A. Mayer, V. Balasubramanian, T. Mora, and A. M. Walczak, Proc. Nat. Acad. Sci. USA **112**, 5950 (2015).
[17] G. Zhang, F. H. Stillinger, and S. Torquato, J. Chem. Phys **145**, 244109 (2016).
[18] D. Chen and S. Torquato, Acta Mater. **142**, 152 (2018).
[19] Y. Xu, S. Chen, P.-E. Chen, W. Xu, and Y. Jiao, Phys. Rev. E **96**, 043301 (2017).
[20] B.-Y. Wu, X.-Q. Sheng, and Y. Hao, PLoS ONE **12**, e0185921 (2017).
[21] A. Chremos and J. F. Douglas, Ann. Phys. **529**, 1600342 (2017).
[22] B. Jancovici, Phys. Rev. Lett. **46**, 386 (1981).
[23] E. Lomba, J.-J. Weis, and S. Torquato, arXiv:1710.06806.
[24] A. Bhatia and D. Thornton, Phys. Rev. B **2**, 3004 (1970).
[25] J.-P. Hansen and I. McDonald, *Theory of Simple Liquids*, 2nd ed. (Academic, London, 1990).
[26] J.-P. Hansen and P. Vieillefosse, Phys. Rev. Lett. **37**, 391 (1976).
[27] F. Lado, Phys. Rev. B **17**, 2827 (1978).
[28] M. Baus and J.-P. Hansen, Phys. Rep. **59**, 1 (1980).
[29] J. M. Caillol, D. Levesque, J. J. Weis, and J. P. Hansen, J. Stat. Phys. **28**, 325 (1982).
[30] F. Saija and P. V. Giaquinta, J. Chem. Phys. **117**, 5780 (2002).
[31] N. G. Almarza, C. Martín, E. Lomba, and C. Bores, J. Chem. Phys. **142**, 014702 (2015).
[32] E. Lomba, J. J. Weis, and F. Lado, J. Chem. Phys. **127**, 074501 (2007).
[33] P. V. Giaquinta and G. Giunta, Physica A **187**, 145 (1992).
[34] T. M. Truskett, S. Torquato, and P. G. Debenedetti, Phys. Rev. E **62**, 993 (2000).
[35] S. Leeuw and J. W. Perram, Physica A **113**, 546 (1982).
[36] D. P. Landau and K. Binder, *A Guide to Monte Carlo Simulations in Statistical Physics* (Cambridge University Press, Cambridge, 2005).
[37] J. Salas and A. D. Sokal, J. Stat. Phys. **98**, 551 (2000).